Journal of Alloys and Compounds 503 (2010) 449–453

Contents lists available at ScienceDirect

Journal of Alloys and Compounds

journal homepage: www.elsevier.com/locate/jallcom

Rod-like ferrites obtained through thermal degradation of a molecular ferrimagnet

A. Bhattacharjee[a,*], D. Roy[a], M. Roy[b], S. Chakraborty[b], A. De[c], J. Kusz[d], W. Hofmeister[e]

[a] Department of Physics, Visva-Bharati University, Siksha Bhavan, Santiniketan 731235, India
[b] Microelectronics Division, Saha Institute of Nuclear Physics, Kolkata, India
[c] Department of Physics, Presidency College, Kolkata, India
[d] Institute of Physics, University of Silesia, Katowice, Poland
[e] Institut für Geowissenschaften der Universität, Mainz, Germany

ARTICLE INFO

Article history:
Received 7 August 2009
Received in revised form 4 May 2010
Accepted 5 May 2010
Available online 13 May 2010

Keywords:
Molecular magnet
Thermal degradation
Ferrite

ABSTRACT

This paper presents the characteristics of iron oxides obtained through thermal degradation of a molecular ferrimagnet, $\{N(n\text{-}C_4H_9)_4[Fe^{II}Fe^{III}(C_2O_4)_3]\}_\infty$ and sheds light on the reaction pathways of degradation. The powder XRD pattern and the IR spectra of the degraded material reveal the formation of hematite. The SEM study exhibits that the degraded material consists of rod-like crystals of average length and diameter being 350 and 140 nm, respectively. But the mean crystallite size as estimated from the XRD pattern analysis is 169(2) nm. The magnetization study of the degraded material by SQUID shows the presence of Morin and Verwey transitions. Formation of ferrites through thermal degradation of the molecular magnetic precursor is further established by thermogravimetric study of the precursor. This is the first ever report of synthesis of nano-ferrites from a molecular magnet precursor, which underlines a new route for synthesis of ferrites.

1. Introduction

In recent years magnetic nanoparticles have been the subject of intense basic and technological research [1–6]. Among different synthetic routes for preparation of metal oxide nanoparticles, the technique of preparing such nanoparticles through thermal degradation of metal complexes becomes increasingly important mainly due to easy control of process conditions, purity, phase, composition, microstructure, etc. of the resultant products [7,8]. The thermal degradation technique was first reported in 1870 [9]. The formation of mixed-metal oxides was reported as a main product in the case of solid state thermal degradation of bimetallic oxalate precursors [10,11]. Polymeric bimetallic oxalate complexes of formula, $\{A[M^{II}M^{III}(C_2O_4)_3]\}_\infty$, ($M^{II}$, M^{III}: di-/trivalent transition metal ions; C_2O_4: oxalate ligand) [12] have also been important topics in the field of molecular magnetism [13]. Recent report [14] showed that thermal degradation of a ferrimagnetic material, $\{N(n\text{-}C_4H_9)_4[Mn^{II}Cr^{III}(C_2O_4)_3]\}_\infty$ results in a spinel compound, $Mn_{1.5}Cr_{1.5}O_4$ at ~500 °C and under suitable conditions both the metals in such heterometallic molecular complexes, if used as precursor, can be transformed into metal oxides. Furthermore, the synthesis of $\{A[M^{II}M^{III}(C_2O_4)_3]\}_\infty$ type molecular magnetic materials as precursors for thermal degradation is quite easy and economic, and the desired metal oxides can be prepared from such heterometallic oxalate complexes at relatively low temperatures. In this light, it was felt interesting to explore the thermal behavior of some widely studied heterometallic molecular anti-/ferrimagnetic material precursors of $\{A[M^{II}M^{III}(C_2O_4)_3]\}_\infty$ family. In the present study, a molecular precursor, $\{N(n\text{-}C_4H_9)_4[Fe^{II}Fe^{III}(C_2O_4)_3]\}_\infty$ [15], a molecular ferrimagnet with Néel temperature = 43.5 K is taken to form the iron oxides through thermal degradation and develop a convenient and economic route for the preparation of such technologically important oxide materials. Precisely, the fine powdery precursor material, $\{N(n\text{-}C_4H_9)_4[Fe^{II}Fe^{III}(C_2O_4)_3]\}_\infty$ was synthesized at room temperature through usual laboratory method that forms rod-like iron oxides on thermal degradation. This is probably the first time when rod-like iron oxide crystals were synthesized by thermal degradation of a molecular magnetic material.

2. Experimental

The precursor, $\{N(n\text{-}C_4H_9)_4[Fe^{II}Fe^{III}(C_2O_4)_3]\}_\infty$ (BuFeFe in short) was prepared in one pot reaction following the procedures reported by Ōkawa et al. [12]. The powdery material thus obtained, was then loaded into a furnace at 750 °C for 10 h for its thermal degradation. The X-ray powder diffraction on the thermally degraded material was performed with a Seifert's powder diffractometer (XRD 3000 TT) equipped with a Cu Kα radiation source, and the Full Proof program was used for the data analysis. The scanning electron microscopy (SEM, model: FEI Quanta 200F) was employed to study the morphology of the grown and degraded materi-

* Corresponding author.
E-mail address: ashis.bhattacharjee@visva-bharati.ac.in (A. Bhattacharjee).

0925-8388/$ – see front matter © 2010 Elsevier B.V. All rights reserved.
doi:10.1016/j.jallcom.2010.05.031

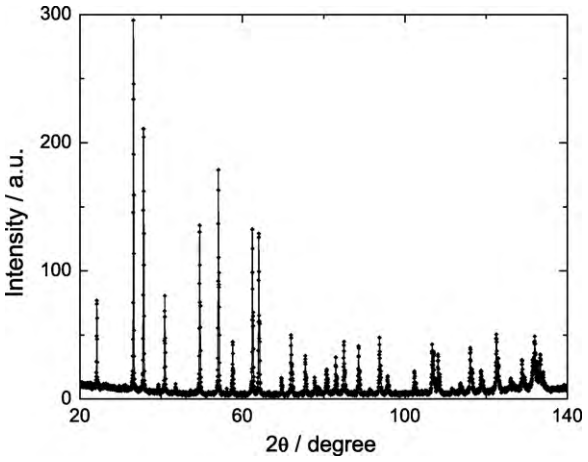

Fig. 1. Powder XRD pattern of the degraded product of $\{N(n\text{-}C_4H_9)_4[Fe^{II}Fe^{III}(C_2O_4)_3]\}_\infty$.

als. The IR spectrum of the degraded material was obtained by SPECTRUM RX1 FTIR of PerkinElmer with KBr supported sample wafer. The magnetic measurement of the sample was carried out by Quantum Design's MPMS XL SQUID magnetometer. The grown material was used for thermogravimetric analysis (TGA) using a thermogravimetric analyzer (Nietzsche, Germany, model: STA 449C) at a heating rate of 5 °C/min.

3. Results and discussion

3.1. Characterization of iron oxide obtained on thermal degradation

The X-ray powder diffraction (XRD) pattern of the thermally degraded sample (say, FeFe) obtained using Cu Kα line within $20° < 2\theta < 140°$ range, is shown in Fig. 1. The pattern clearly exhibits that all diffraction peaks/lines correspond to hematite (JCPDF no. 24-72 and 13-534) with unit cell parameters $a = b = 5.03286$ Å; $c = 13.74430$ Å, $\alpha = \beta = \gamma = 90.0°$. It is also possible that a small quantity of magnetite is present in the FeFe sample, and in that case the most intense Bragg peak of magnetite to be observed in the XRD pattern would overlap with the Bragg peaks for hematite (JCPDF no. 4-755). From the XRD peak broadening the mean crystallite size (D) of FeFe was estimated using Scherer formula [16]. The estimated value of D is 169(2) nm. This result establishes that nano-sized ferrite particles were formed on thermal degradation of the molecular precursor, BuFeFe.

Surface morphology and particle nature of the precursor as well as the thermally degraded material were observed by SEM. Fig. 2(a) represents the SEM picture of the precursor, whereas Fig. 2(b) represents that of FeFe material. Fig. 2(a) indicates that the precursor BuFeFe contains fine powders. Fig. 2(b) clearly shows that oxides formed (FeFe) on thermal degradation of BuFeFe are the agglomeration of tiny rods having length ranging between 580 and 210 nm and diameter between 210 and 110 nm. While estimated for a large number of specimens, it is found that although there is a small variation in length and breadth of the nanorods, the majority of the rods appear with length and breadth of ~320 and ~110 nm, respectively. However, the estimated mean diameter (140 nm) of the nanorods is very close to the mean crystallite size (169 nm) observed through the powder XRD study of FeFe.

The composition of FeFe was investigated by the IR spectroscopy. The IR spectrum of FeFe illustrated in Fig. 3 shows several distinct bands that allow unequivocal identification of hematite in FeFe. The strong bands at ~542 and ~472 cm^{-1} and weaker band at ~610 cm^{-1} are in good agreement with the IR spectra of hematite [17,18]. No peak corresponding to C=O stretching vibration at ~1632 cm^{-1} is observed in the IR spectrum, which confirms that the precursor containing oxalate ligand is completely decomposed.

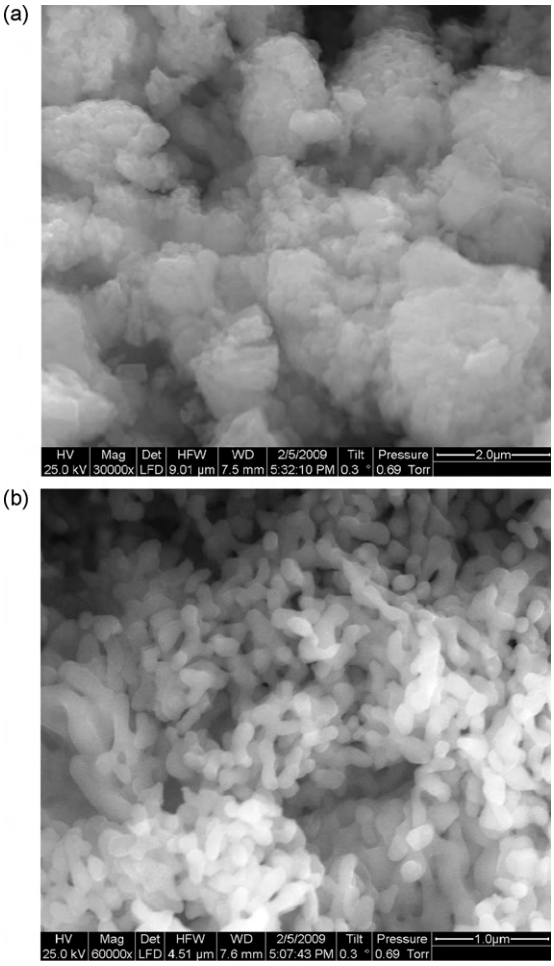

Fig. 2. SEM picture of (a) precursor material, $\{N(n\text{-}C_4H_9)_4[Fe^{II}Fe^{III}(C_2O_4)_3]\}_\infty$, and (b) thermally degraded material – FeFe.

The magnetic behavior of the degraded product, FeFe, which is of great importance for practical applications, was investigated. Fig. 4 shows the temperature dependence of magnetization (M) obtained during two consecutive thermal cyclings in 300–2–300 K range under 1 kOe magnetic field. The $M(T)$ plot during the 1st cooling (1) down from room temperature shows a sharp drop in

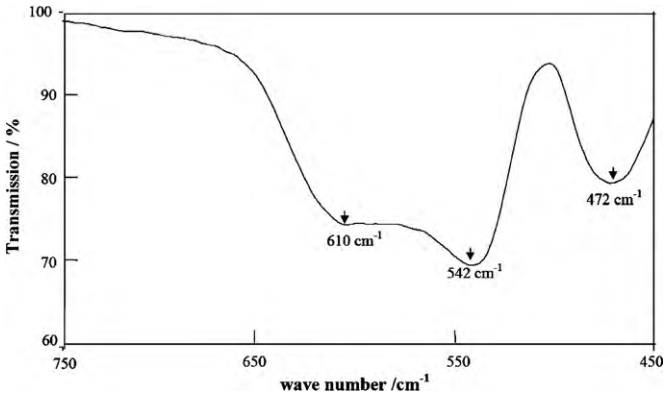

Fig. 3. IR spectra between 450 and 850 cm^{-1} of the degraded product of $\{N(n\text{-}C_4H_9)_4[Fe^{II}Fe^{III}(C_2O_4)_3]\}_\infty$.

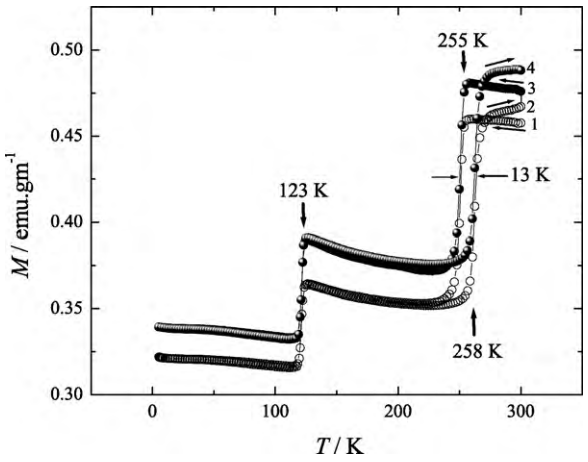

Fig. 4. Temperature dependence of magnetization of the degraded product of. $\{N(n\text{-}C_4H_9)_4[Fe^{II}Fe^{III}(C_2O_4)_3]\}_\infty$ in two successive thermal cycles: cooling (1) → heating (2) → cooling (3) → heating (4). Arrows are guide to the eyes.

magnetization values at 255 K, which continues till 248 K. Below this temperature the $M(T)$ values slowly increase till 123 K. At 123 K the $M(T)$ plot once again suffers a sudden decrease followed by a very gradual increase in $M(T)$ values until 2 K. While heating (2) above 2 K, $M(T)$ plot retraces the same path as seen while cooling till ~233 K, but then rapidly increases beyond ~255 K. Beyond 268 K, $M(T)$ values again increase slowly with increasing temperature up to 300 K. On immediate start of the cooling below this temperature a significant jump appears in the $M(T)$ value at 300 K as a result of which the $M(T)$ plots during the 2nd cooling (3) and 2nd heating (4) shift upwards almost in parallel. As a whole the nature of the $M(T)$ plots during the second cooling–heating cycle remains analogous to those observed during the first cooling-heating cycle. In both the cases of thermal cycling a thermal hysteresis loop of 13 K width in the $M(T)$ plots, associated with a sharp change in $M(T)$ values and centered around ~262 K, is observed. Another sharp transition at ~123 K but without any thermal hysteresis is also noticed.

Fig. 5 shows the field dependence of the isothermal magnetization M in ±70 kOe range at 300 K. Absence of the saturation magnetization as well as the existence of the hysteresis loop at 300 K should be noticed. A narrowing in the hysteresis loop along

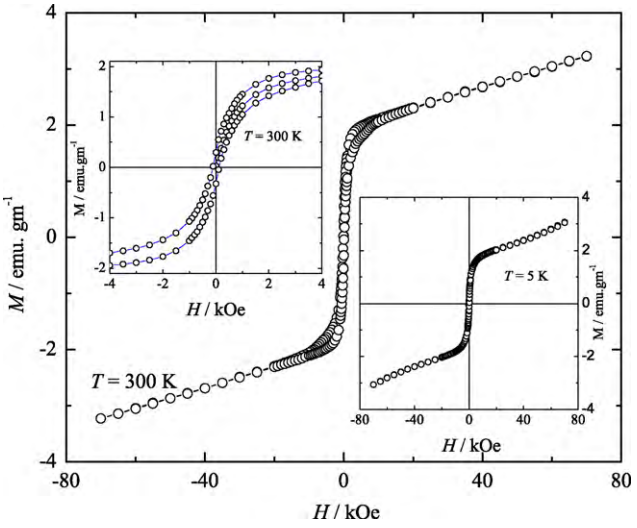

Fig. 5. Magnetic field dependence of magnetization for the degraded product of $\{N(n\text{-}C_4H_9)_4[Fe^{II}Fe^{III}(C_2O_4)_3]\}_\infty$ at 300 K. The left inset shows the low field magnetization behavior, whereas the right inset shows the field dependence at 5 K.

the magnetization axis at low applied field is observed (Fig. 5, left inset). The magnetization curve obtained at 5 K is less hysteretic than that seen at 300 K (Fig. 5, right inset). The values of the coercive field (H_C), remnant magnetization (M_r) and saturation magnetization (M_S) noted from the $M(H)$ plots are 115 and 167 Oe, 0.30 and 0.29 emu · g^{-1}, and 4 and 3.49 emu · g^{-1} at 300 and 5 K, respectively. The values of M_S are determined by extrapolating $1/H$ to zero-field in the M vs. $1/H$ plot based on the high field data. The shape of the hysteresis loops at 5 K and 300 K remains almost the same but it differs slightly from the estimated saturation magnetization M_S values. However, the M_S values at 5 and 300 K are quite comparable, if the uncertainties involved in determination are taken into account, which may indicate the presence of comparable amount of hematite and magnetite in the degraded sample. Mössbauer spectroscopic study of the sample which is underway will be able to estimate the composition of the different magnetic phases present in this material.

From the XRD study it is expected that the present compound should be a hematite. It is well known that a phase transition from a weakly ferromagnetic to an antiferromagnetic state on cooling below the Morin temperature (T_M = 260 K) occurs in hematite [19]. This is a magnetic phase transition in hematite where the antiferromagnetic ordering is reorganized from being aligned perpendicular to the c-axis to be aligned parallel to the c-axis below T_M. Morin transition is a yardstick for hematite materials. Thus, the sharp change in $M(T)$ values and occurrence of a thermal hysteresis centered at 262 K illustrated in Fig. 4 correspond to the Morin transition of the degraded material. This observation confirms that the degraded material contains hematite nanoparticles. Particle shape, size, crystallinity, and surface condition affect the temperature of Morin transition [20]. With consecutive thermal cyclings, i.e., cooling (1) → heating (2) → cooling (3) → heating (4) there has been a constant (~2%) increase in magnetization values recorded at 300 K. These irreversible changes observed in magnetization values for FeFe with repeated thermal cyclings may be interpreted in terms of domain reorganization [21]. It is known that the thermal cycling through Morin temperature changes the domain configuration of hematite. The saturation remanence of hematite is usually only partly recovered upon cycling. Domain structure in its saturation remanent state shows that the most of the crystals loose their domain pattern on cooling [22,23]. Below the Morin temperature, a single-domain state is often observed, and if they are warmed to room temperature again, a new pattern is seen. A charge-ordering transition, first observed by Verwey, occurs in magnetite, Fe_3O_4 ($Fe^{3+}[Fe^{3+}Fe^{2+}]O_4$) in which an ordering of Fe^{3+} and Fe^{2+} ions within octahedral sites is thought to occur below $T_V \approx 120$ K [24]. A sharp drop in magnetization at 120 K due to Verwey transition is the usual fingerprint to identify magnetite [25,26]. Interestingly, the sharp jump in $M(T)$ plots at ~123 K shown in Fig. 4 indicates the presence of magnetite in FeFe. Thus, the presence of both the hematite and magnetite in the FeFe material obtained on thermal degradation of a single-molecular magnetic precursor is confirmed by the two fingerprints – the Morin and Verwey transitions recorded in the present study through magnetic measurements. The present XRD study of FeFe can detect only its hematite structure, whereas the magnetic study establishes the presence of hematite as well as magnetite within FeFe. The magnetite phase is not seen in the XRD pattern as its most intense peak overlapped with the intense peak of the dominant hematite phase. Thermal degradation of iron oxalate to hematite in air atmosphere and to magnetite in presence of CO/CO_2 mixture are reported by other workers [11]. In the present case, inside the furnace the thermal degradation initially started in air atmosphere leading to the formation of hematite along with profuse amount of CO_2 and subsequently, on further heating it might have led to the formation of magnetite [11].

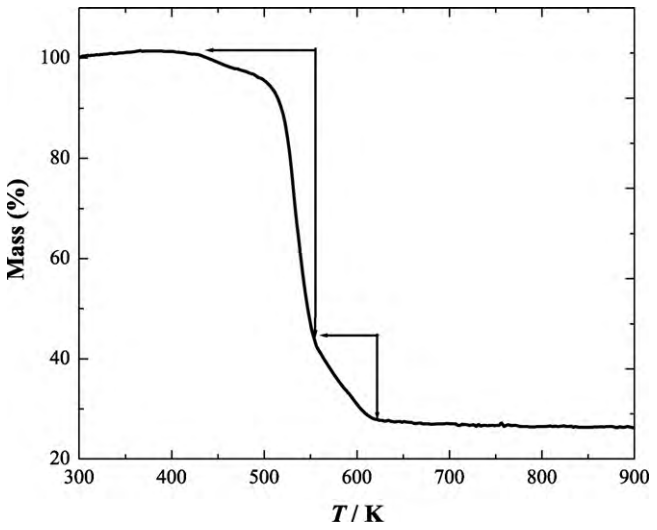

Fig. 6. Thermogravimetry profile at 5 °C/s heating rate of $\{N(n\text{-}C_4H_9)_4[Fe^{II}Fe^{III}(C_2O_4)_3]\}_\infty$. Arrows are guide to the eyes.

3.2. Formation of ferrites through thermal degradation

Thermal degradation of the precursor BuFeFe in presence of dry nitrogen gas at a heating rate of 5 °C/min is monitored by thermogravimetry (TG) and shown in Fig. 6. The degradation proceeds through intermediate phases, and finally results into the formation of a powdery red-product FeFe. A mass loss sets in at ~430 K and is almost completed at 620 K. The degradation occurs in two-steps – 1st step: 430–550 K and 2nd step: 550–620 K. No further change in mass loss was recorded in the TG profile above 620 K up to 970 K. The thermal degradation may proceed by internal redox pathway [14]. Two possible reaction pathways are prescribed through the equations given below:

$$\text{Pathway I}: 3\{N(n\text{-}C_4H_9)_4[Fe^{II}Fe^{III}(C_2O_4)_3]\}_\infty \rightarrow 2Fe_3O_4(s) + 3(n\text{-}C_4H_9)_3N(g) + 3C_4H_8(g) + 10CO_2(g) + 8CO(g) + (3/2)H_2(g) \quad (a)$$

$$\text{Pathway II}: \{N(n\text{-}C_4H_9)_4[Fe^{II}Fe^{III}(C_2O_4)_3]\}_\infty \rightarrow Fe_2O_3(s) + (n\text{-}C_4H_9)_3N(g) + C_4H_8(g) + 3CO_2(g) + 3CO(g) + (3/2)H_2(g) \quad (b)$$

where 'g' and 's' denote gaseous and solid substances, respectively. The observed mass loss for the 1st step is 55%, whereas that for the 2nd step is 21.2%. Following the above reaction pathways, the calculated values of mass loss for the 1st and 2nd steps in the TG profile are 52.8 and 21.4% for pathway II, whereas those for the pathway I are 53.6 and 21.4%, respectively, which correspond to the observed values of mass loss from the TG curve. Thus, the proposed reaction pathways indicate the formation of either Fe_3O_4 (magnetite) or Fe_2O_3 (hematite) or a mixture of both as a result of degradation of the precursor, BuFeFe completed at 620 K. It is highly probable that hematite thus formed will be slowly converted to magnetite when heated at higher temperatures [27]. This is in an excellent agreement with the predictions of the formation of iron oxides (hematite and/or magnetite) through thermal degradation of the molecular precursor as evident in the magnetic study as well as the IR spectroscopy.

The thermal degradation, as represented by the two reaction pathways described above, involve the removal of gaseous substances butane (C_4H_8), carbon dioxide (CO_2), carbon monoxide (CO), $(n\text{-}C_4H_9)_3N$ and a minute amount of H_2 in the 1st step of the degradation process, whereas the 2nd step results in due to further degradation associated with removal of more CO_2 gas. All the by-products (gaseous substances) during this thermal degradation process are volatile and hence easily removed from the product, which offers a distinct advantage in the synthesis.

4. Conclusions

Present study illustrates that a two-step thermal degradation process of a molecular ferrimagnetic precursor, $\{N(n\text{-}C_4H_9)_4[Fe^{II}Fe^{III}(C_2O_4)_3]\}_\infty$ may result into the formation of nano-sized ferrite rods. The average length and diameter of the nanorods estimated from the SEM picture are 350 and 140 nm, respectively. The aspect ratio (length divided by width) of the nanorods is ~2.6 which is well within the range that is expected for nanorods. The formation of ferrites as seen through TG profile is complemented by the results of XRD, SEM, IR and SQUID studies. It is desirable to interrupt the reaction process (TG) at intermediate temperatures and characterize the physical/chemical nature of the products thus obtained. In this light, further studies are in progress to explore any effect of heating rate, temperature range of heating, ambience, etc. on the shape and size of rods formed, and to study the parameters controlling the phase of the thermally degraded material. Studies on various precursor materials during the thermal degradation and the mechanism of degradation kinetics are presently under our investigation.

The present work completely agrees with the results obtained by Neo et al. [14] and suggests that the oxalate-based mixed-metal molecular complexes are suitable single-molecular precursors to composite metal oxides. Thermal degradation of oxalate to oxide with no interfering solid by-products might be a highly desirable outcome. An important conclusion can be drawn from this work is that the metal oxide products synthesized from 'molecular-to-material' pathway are nano-structured material.

Acknowledgement

For this work a research grant (Project No. SR/S2/CMP-0036/2006) from the Department of Science & Technology, New Delhi, India (to AB) is gratefully acknowledged.

References

[1] J.P. Reithmaier, P. Petkov, W. Kulisch, C. Popov (Eds.), Nanostructured Materials for Advanced Technological Applications (NATO Science for Peace and Security Series B: Physics and Biophysics), Springer, 2008.
[2] D. Gatteschi, R. Sessoli, J. Villain, Molecular Nanotechnology, Mesoscopic Physics and Technology, Oxford University Press, 2006.
[3] M.L. Kahn, A. Glaria, C. Pages, M. Monge, L.S. Macary, A. Maisonnat, B. Chaudret, J. Mater. Chem. 19 (2009) 4044–4060.
[4] W. Zhou, K. Tang, S. Zeng, Y. Qi, Nanotechnology 19 (2008) 65602–65610.
[5] S. Mukherjee, A.K. Pal, S. Bhattacharya, S. Chattopadhyay, J. Phys.: Condens. Matter 20 (2008) 55204–55215.
[6] S. Chakravorty, M. Bandyopadhyay, J. Phys.: Condens. Matter 19 (2007) 216201–216216.
[7] Y.C. Zhang, J.Y. Tang, X.Y. Hu, J. Alloys Compd. 462 (2008) 24–28.
[8] X. Wu, J. Tang, Y. Zhang, H. Wang, Mater. Sci. Eng. B 157 (2009) 81–86.
[9] E.J. Maumene, Bull. Soc. Chim. 13 (1870) 194–197.
[10] N. Deb, J. Anal. Appl. Pyrol. 87 (2010) 269–275.
[11] A. Angermann, J. Töffer, J. Mater. Sci. 43 (2008) 5123–5130.
[12] H. Ōkawa, N. Matsumoto, H. Tamaki, S. Kida, M. Ohba, Mol. Cryst. Liq. 233 (1993) 257–262.
[13] J.S. Miller, M. Drillon (Eds.), From Molecules to Materials IV, Wiley-VCH, Weinheim, 2003.
[14] K.E. Neo, Y.Y. Ong, H.V. Huynh, T.S. Andy Hor, J. Mater. Chem. 17 (2007) 1002–1006.
[15] A. Bhattacharjee, S. Reiman, V. Ksenofontov, P. Gütlich, J. Phys.: Condens. Matter 15 (2003) 5103–5112.
[16] B.D. Cullity, Elements of X-Ray Diffraction, Addison-Wesley, Reading, MA, 1956, p. 99.
[17] B. Gillot, Vib. Spectrosc. 6 (1994) 127–148.

[18] G.N. Kustova, E.B. Burgina, V.A. Sadykov, S.G. Poryvaev, Phys. Chem. Miner. 18 (1992) 379–382.
[19] F.J. Morin, Phys. Rev. 78 (1950) 819–820.
[20] R.D. Zysler, D. Fiorani, A.M. Testa, M. Godinho, E. Agostinelli, L. Suber, J. Magn. Magn. Mater. 272 (2004) 1575–1576.
[21] C.B. De Boer, T.A.T. Mullender, M.J. Dekker, Geophys. J. Int. 146 (2001) 201–216.
[22] J.A. Eaton, A.H. Morrish, J. Appl. Phys. 40 (1969) 3180–3185.
[23] A.H. Morrish, Canted Antiferromagnetism: Hematite, World Scientific, London, 1994.
[24] E.J. Verwey, Nature 144 (1939) 327–328.
[25] R.M. Cornell, U. Schwertmann, The Iron Oxides, VCH, Wienheim, 1996.
[26] P. Piekarz, K. Parlinski, A.M. Oles, Phys. Rev. B 76 (2007) 165124–165139.
[27] I.S. Lyubutin, C.R. Lin, Y.V. Korzhetskiy, T.V. Dmitrieva, R.K. Chiang, J. Appl. Phys. 106 (2009) 34311–34316.